Carbon Monoxide in low-mass dwarf stars

Hugh R. A. Jones[1,2], Yakiv Pavlenko[3], Serena Viti[4], R.J. Barber[4], Larisa A. Yakovina[3], David Pinfield[1], Jonathan Tennyson[4]

[1] *Centre for Astrophysics Research, University of Hertfordshire, College Lane, Hatfield, Hertfordshire AL10 9AB*
[2] *Astrophysics Research Institute, Liverpool John Moores University, Twelve Quays House, Egerton Wharf, Birkenhead CH41 1LD*
[3] *Main Astronomical Observatory of Academy of Sciences o Ukraine, Golosiiv woods, Kyiv-127, Ukraine 03680*
[4] *Department of Physics and Astronomy, University College London, Gower Street, London WC1E 6BT*

ABSTRACT
We compare high resolution infrared observations of the CO 3-1 bands in the 2.297–2.310 μm region of M dwarfs and one L dwarf with theoretical expectations. We find a good match between the observational and synthetic spectra throughout the 2000-3500K temperature regime investigated. Nonetheless, for the 2500-3500 K temperature range the temperatures that we derive from synthetic spectral fits are higher than expected from more empirical methods by several hundred K. In order to reconcile our findings with the empirical temperature scale it is necessary to invoke warming of the model atmosphere used to construct the synthetic spectra. We consider that the most likely reason for the back-warming is missing high temperature opacity due to water vapour. We compare the water vapour opacity of the Partridge & Schwenke (1997) line list used for the model atmosphere with the output from a preliminary calculation by Barber & Tennyson (2004). While the Partridge & Schwenke line list is a reasonable spectroscopic match for the new line list at 2000 K, by 4000 K it is missing around 25% of the water vapour opacity. We thus consider that the offset between empirical and synthetic temperature scales is explained by the lack of hot water vapour used for computation of the synthetic spectra. For our coolest objects with temperatures below 2500 K we find best fits when using synthetic spectra which include dust emission. Our spectra also allow us to constrain the rotational velocities of our sources, and these velocities are consistent with the broad trend of rotational velocities increasing from M to L.
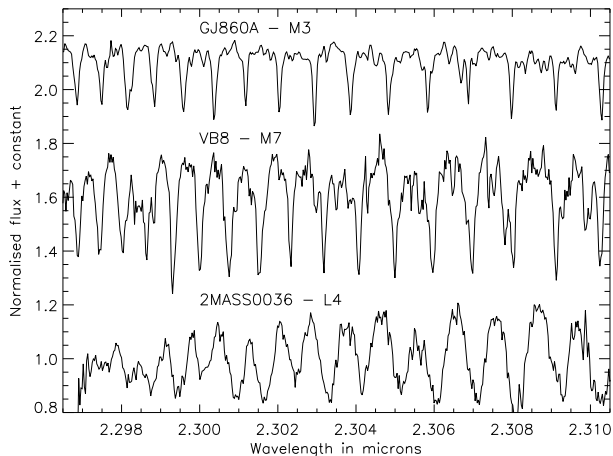
Key words: binaries: infrared– optical– stars: fundamental parameters – stars: atmospheres – stars: late type – stars: population II; brown dwarfs

1 INTRODUCTION

Low mass dwarf stars dominate our Galaxy in terms of number. They provide a probe of our understanding of main sequence stellar evolution and are the key in determining the boundary between stellar and sub-stellar objects. There are relatively few observations of known-mass low mass stars. Parameters such as effective temperature and metallicity, vital in determining positions in H-R diagrams, remain controversial. To reliably constrain the low-mass initial stellar mass function it is essential to know the basic properties of standard low-mass M, L and T dwarfs. A correct determination of the mass function relies on an accurate transformation from luminosity and temperature to mass. These relationships are sensitive to the stellar chemical composition. For hotter objects colour-colour diagrams are reason-

ably reliable indicators of temperature and metallicity. However such diagrams for low mass dwarfs do not yet reproduce the broadband fluxes within a reasonable error and therefore cannot be uniquely used to determine reliable temperatures, metallicities and gravities. Ideally it would be useful to have spectroscopic signatures sensitive to temperature, metallicity and gravity that are reproducible with synthetic spectra.

Many authors have determined the properties of low-mass objects using synthetic spectra. However, the use of such synthetic spectra are problematic because (1) the objects are dominated by various diatomic and triatomic molecules whose high temperature properties are poorly understood and (2) the large number of different transitions means that most transitions are substantially blended with other competing opacities. One potential route to resolve these issues is to try to find spectral regions where these is-

Figure 1. Spectral sequence of CO bands from M3 to L4.
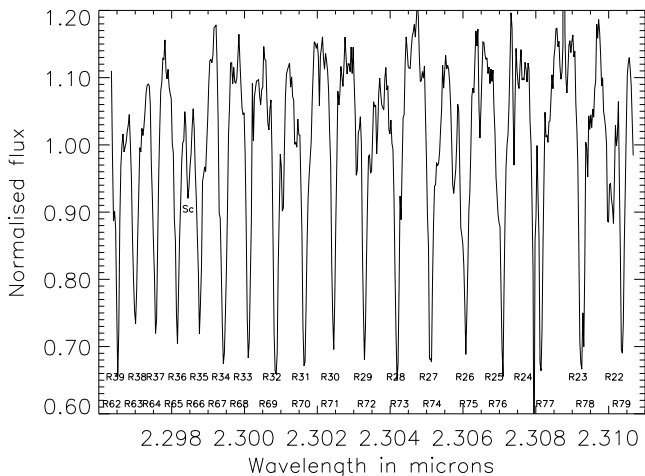
Figure 2. CO 3-1 transitions and Sc line identified in GJ752B. The resolution of the data is insufficient to unambiguously identify the higher energy (R62 to R79). The R24 and R77 transistions appear to be resolved from one another, however, inspection of Fig. 3 indicates that the left-hand feature is due to water vapour.

sues are less problematic. For example the middle of the J-band window is a promising region (Jones et al. 1996; McLean et al. 2003). Although this region is relatively transparent and is in a wavelength regime where infrared spectrometers are relatively sensitive it does have shortcomings. In addition to the problems with modelling water vapour at short wavelengths (Jones et al. 2002), it is now clear that the poorly modelled opacities of FeH (Cushing et al. 2003), as well as VO and TiO (McGovern et al. 2004) also play an important role in this region.

Here we investigate an alternative wavelength regime. In the spectral region between 2.29 and 2.45 μm, CO is a key opacity for low mass stars. CO appears in a relatively easily-observed stable part of the K band and molecular data, including f-values, are well known. Moreover,
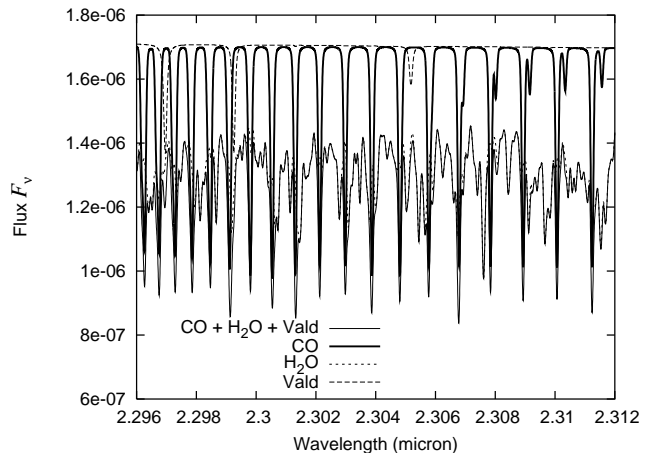
Figure 3. The plot shows the various opacity contributions for a 3000 K log g=5.0 solar metallicity model from atomic lines (top of plot, dashed line), carbon monoxide transitions (top of the plot, thick solid line), water vapour (dotted line) and the overall formation of the continuum primarily dominated by water (thin solid line).

CO is believed to be formed under LTE (e.g. Carbon et al. 1976) and therefore the levels are populated according to the Boltzmann distribution. The available CO line list has proven to be reliable for solar work and so is believed to be more than adequate for the lower energy states accessed in cool dwarf atmospheres (Goorvitch 1994). The other significant metal diatomic species appearing in infrared cool dwarf stars are FeH, VO and TiO, however, these diatomics are not as prominent as CO at wavelengths obtainable with the infrared echelle used for these observations.

In Pavlenko & Jones (2002) we showed that the $\Delta\nu$=2 carbon monoxide bands around 2.3–2.4 μm can be well modelled by synthetic spectra. This region is dominated by CO and H_2O bands, and has few atomic lines of significance. This is advantageous because CO is well modelled relative to the current quality of atomic oscillator strengths in the infrared (e.g. Jones et al. 1996, Lyubchik et al. 2004). Here we extend this work to much higher resolution, where the CO bands are very distinct from the water vapour modelled continuum. The wavelength range (2.297 to 2.311 microns) was chosen on the basis of features in late type dwarf spectra identified to be relatively metallicity sensitive and reproducible by synthetic spectra in Viti et al. (2002).

2   OBSERVATIONS

The targets chosen for this study are all bright relatively well-studied M and L dwarfs. The source selection was made in order to give good coverage in spectral type and metallicity. However, the half nights available to us limited our sample to a relatively restricted range of right ascension. The sample is shown in Table 1.

The targets were observed during the first half of the nights of 2001 September 8–12 with the Cooled Grating Spectrometer 4 (CGS4) on the UK Infrared Telescope (UKIRT) on Mauna Kea, Hawaii. The weather was photometric throughout with optical seeing of typically 0.8".

Table 1. Literature properties of observed targets: kinematic classification (KIN-class) are from Leggett (1992) and Leggett et al. (1998), spectral types are from Kirkpatrick, Henry & McCarthy (1991) and Gizis (2002) and empirical temperatures derived using Lane et al. (2001), Segransan et al. (2003), Dahn et al. (2002) and Vrba et al. (2004).

Object	KIN-class	Sp Type	Empirical temperature (K)
GJ860A	OD	dM3	3310
GJ725A	OD	dM3	3310
GJ725B	OD	dM3.5	3230
GJ896A	YD	dM3.5	3230
G87-9B	–	dM4	3150
GJ699	O/H	dM4	3150
GJ860B	OD	dM4	3150
GJ896B	YD	dM4.5	3070
GJ630.1A	H	dM4.5	3070
GJ166C	OD	dM4.5	3070
GJ2005ABCD	OD	dM5.5	2910
GJ65A	YD	dM5.5	2910
GJ65B	YD	dM6	2825
GJ644C	OD	dM7	2670
GJ752B	OD	dM8	2550
LP944-20	YD	dM9	2440
2MASS0036	-	dL4	1900

Table 2. Derived synthetic spectra parameters are given. The syntax for the models is T_{eff} / log g / [M/H] so for example 2800/5.0/-0.5 means a 2800 K, gravity = 5.0 cm/s and metallicity –0.5 dex model. Rotational velocities are derived from the unconstrained minimisation fit and are typically accurate to 3 km/s. Values given in italic are fixed. The values for the minimisation of coolest objects LP944-20 and 2MASS0036 (shortened its full designation of 2MASS J00361617+1821104) are rather dependent on the details of the model. Minimisations for these objects are presented in Fig. 9.

Object	Rotational velocity v sin i (km/s)	unconstrained minimisation	[M/H] constrained T_{eff} & log g minimisation	T_{eff} constrained [M/H] & log g minimisation
GJ860A	7.0	3500/5.5/0.0	3500/5.5/*0.0*	*3300*/5.0/-1.0
GJ725A	5.0	3500/5.5/-0.5	3600/5.5/*0.0*	*3300*/5.0/-1.5
GJ725B	7.0	3500/5.5/0.0	3500/5.5/*0.0*	*3200*/5.0/-1.5
GJ896A	10.0	3400/4.5/-1.5	3600/5.5/*0.0*	*3200*/4.5/-2.0
G87-9B	6.0	3500/4.5/-0.5	3500/5.5/*0.0*	*3200*/5.0/-1.5
GJ699	5.0	3500/4.5/-0.5	3600/5.5/*0.0*	*3200*/4.5/-2.0
GJ860B	8.0	3500/5.5/0.0	3500/5.5/*0.0*	*3200*/4.5/-1.5
GJ896B	15.0	3500/5.0/-0.5	3500/5.5/*0.0*	*3100*/4.5/-2.0
GJ630.1A	27.5	3300/5.0/-0.5	3300/5.0/*0.0*	*3100*/4.5/0.0
GJ166C	5.0	3400/5.5/-0.5	3500/5.5/*0.0*	*3000*/4.5/-2.0
GJ2005ABCD	14.0	3000/5.5/-1.0	3300/4.5/*0.0*	*2900*/5.0/-1.5
GJ65A	31.5	3400/4.5/0.0	3400/4.5/*0.0*	*2900*/5.5/-1.5
GJ65B	29.5	3300/4.5/0.0	3300/4.5/*0.0*	*2800*/5.5/-1.5
GJ644C	12.5	2900/4.5/0.0	2900/4.5/*0.0*	*2700*/5.0/-1.0
GJ752B	10.5	2900/5.5/0.0	2900/5.5/*0.0*	*2600*/5.0/-1.5
LP944-30	31.0	–	–	–
2MASS0036	38.0	–	–	–

Comparison sky spectra were obtained by nodding the telescope so that the object was measured successively in two rows of the array, separated by 30 arcsec.

The echelle grating in 24th order at a central wavelength setting of 2.304 microns was used for all observations. This setup gives wavelength coverage from 2.297 to 2.311 microns at a resolution of approximately 42000.

To remove telluric bands of water, oxygen, carbon dioxide and methane, we observed A and B standard stars. Such stars are not expected to have features in common with cool dwarf stars and appear to be featureless across our spectral range. Wavelength calibration was carried out using a xenon 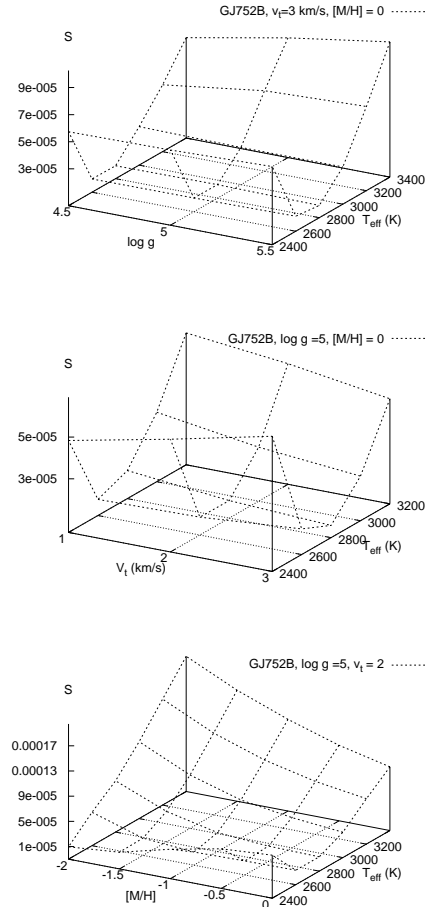arc lamp. This generally worked well because although there are only four lines available in this region, the xenon lines at 2.29 and 2.31 microns fall at either edge of the array and so provide a good wavelength calibration. The only caveat to this is that the wavelength positioning of the echelle is only accurate to around 20 pixels and so the desired wavelength interval is sometimes shifted redward or blueward by around 0.001 microns. Our cross-correlation tests indicate that the wavelength calibration was better than 0.0001 microns. Sky subtraction was done with standard routines which take into account any residual sky emission due to variation of the sky brightness between paired object and sky spectra. The signal was spread between three rows. To extract the spectrum from the sky subtracted signal an Op-
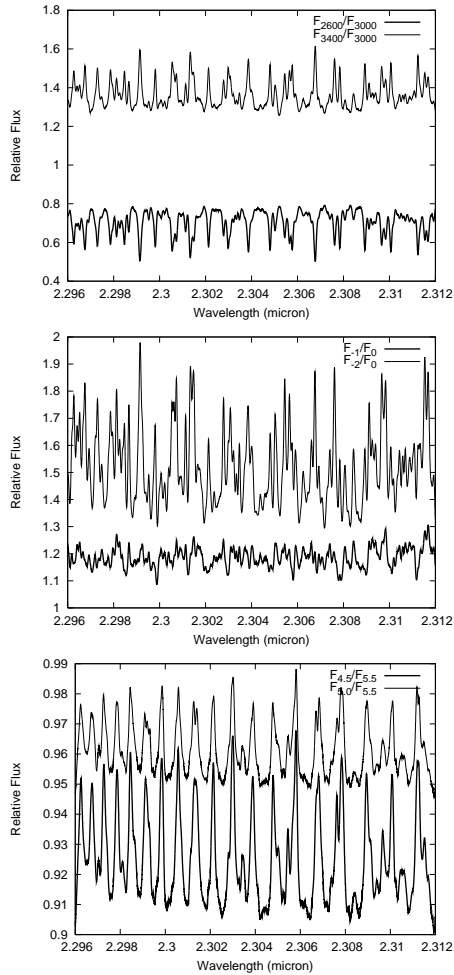
Figure 4. The above plots show the temperature (top), metallicity (middle) and gravity (bottom) dependence of synthetic spectra around a base model of 3000 K, solar metallicity, log g = 5.0. The value of the model atmosphere parameter being adjusted is indicated as subscript. For example in the middle plot, the label F_{-1}/F_0 indicates the flux (F) of a 3000 K, [M/H]=–1, log g = 5.0 model divided by a 3000 K, [M/H]=0, log g = 5.0 model.
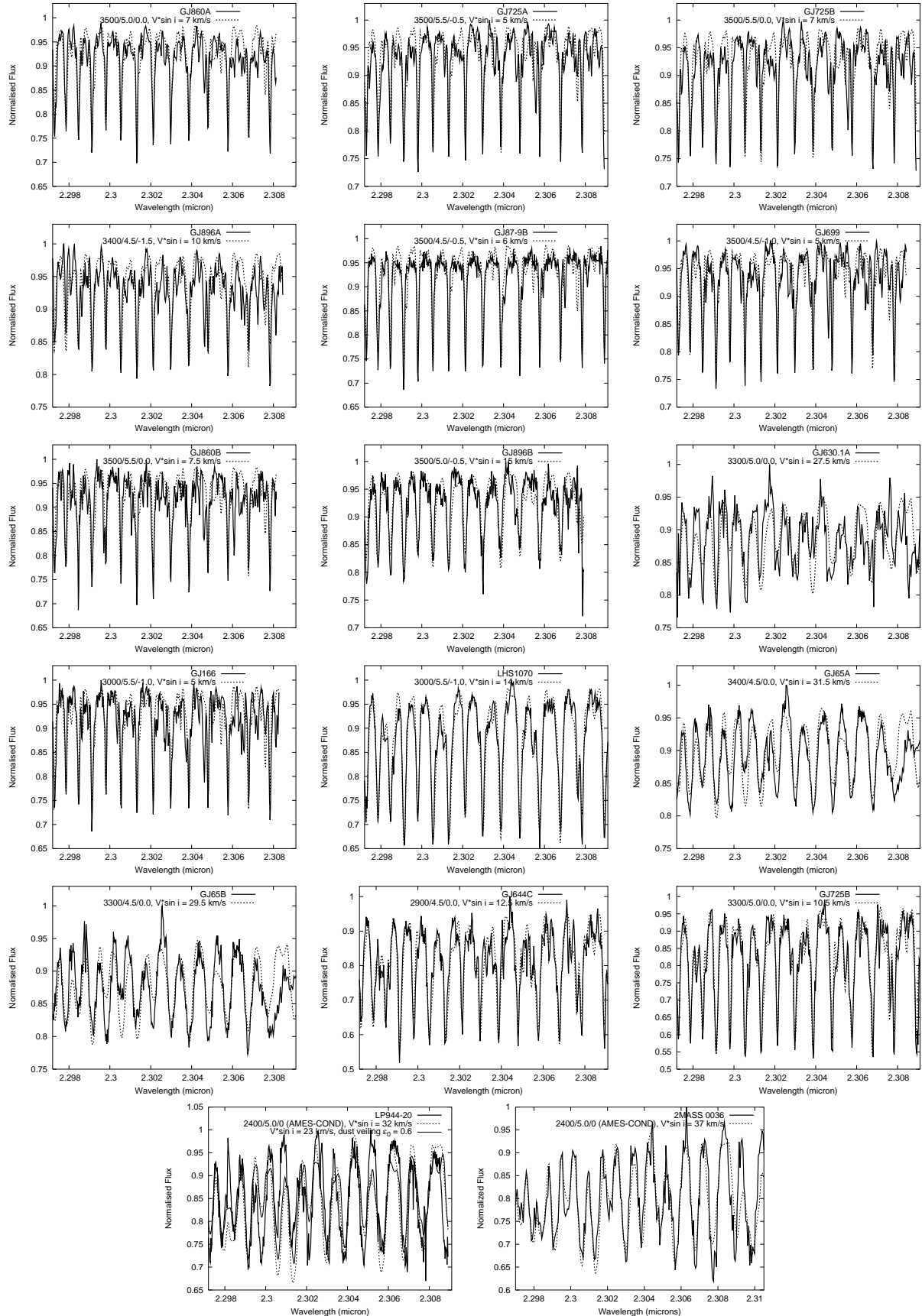

Figure 5. Surface plots showing the sensitivity of the best fit temperature of GJ752B to metallicity, gravity and turbulent velocity. A base model of solar metallicity, log g=5.0 and v_t=3km/s is used.

timal Extraction technique was used; this combines the rows using weights based on the spatial profile of the stellar image. The spectra were reduced using the *Figaro*, *Specdre* and *Kappa* packages provided and supported by Starlink.

A spectral sequence from M3 to L4 is shown in Fig. 1. It can be seen from Figure 2 that individual rotational CO transitions can be resolved in our observed spectra. The CO opacities in our spectra are made up of a large number of spectral lines, covering a wide intensity range, of the second overtone (ν = 2–0). The second overtone band of CO originates from vibration-rotation transitions in the ground electronic state $X^1\Sigma$ and obeys the selection rules $\Delta\nu = 2$ and $\Delta J = \pm1$. The band head of the second overtone (i.e the point at which the separation between the R transitions is zero), occurs at ~ 2.290 μm and therefore both 'hot' (such as R77) and 'cold' (such as R24) rotational transitions are seen in our spectra.

3   THE MODELS

Model atmospheres from the Phoenix code were used for this work. In particular we used the grid known as NextGen (Hauschildt et al. 1999) but also Dusty (Allard et al. 2001) and AMES-COND models (Allard et al. 2001). Model temperatures of 1500 to 3800 K, metallicities of [M/H]= -2.0 to 0.0 and gravities of log g = 4.5 to 5.5 are considered. These parameters represent the probable extremes for the sample based on the literature. We have not tried comparing the system with models computed with non-solar abundance patterns.

Computations of local thermal equilibrium synthetic spectra were carried out by the program WITA6 (Pavlenko 2000). This model assumes LTE, hydrostatic equilibrium for a one-dimensional model atmosphere, and no sources or sinks of energy. The equations of ionisation-dissociation equilibrium were solved for media consisting of atoms, ions and molecules. We took into account ~ 100 components (Pavlenko 2000). The constants for equations of chemical balance were taken from Tsuji (1973). It is worth noting

Figure 6. The observational data are overlaid with the best fit 'unconstrained' synthetic spectra except for LP944-20 and 2MASS0036 for which representative models are shown.

that the chemical balance in cool dwarf atmospheres is governed by the CO molecule (Pavlenko & Jones 2002).

The Partridge & Schwenke (1997: PS) line list is used as the primary source of water vapour lines, though we also made some comparisons with the preliminary line list of Barber & Tennyson (known as BT1, 2004). The partition functions of H_2O were also computed on the PS line list following Pavlenko et al. (2004). We recomputed the constants of dissociation equilibrium using the H_2O partition function following Vidler & Tennyson (2000) though found no significant differences for test synthetic spectra at 3200 K, log $g = 5$ and 2400 K, log $g = 5$ (Pavlenko et al, 2004, in preparation). For CO, we used the $^{12}C^{16}O$ and $^{13}C^{16}O$ line lists of Goorvitch (1994). The CO partition functions were taken from Gurvitz, Weitz & Medvedev (1982). The atomic line list was taken from VALD (Kupka et al. 1999). The relative importance of the different opacities contributing to our synthetic spectra is shown in Fig. 3.

The profiles of molecular and atomic lines are determined using the Voigt function $H(a, v)$, parameters of their natural broadening C_2 and van der Waals broadening C_4 from databases (Kupka et al. 1999) or in their absence computed following Unsold (1955). Owing to the low temperatures in cool dwarf atmospheres, and consequent low electron densities, Stark broadening may be neglected. Computations for synthetic spectra were carried out with a 0.00005 μm step for microturbulent velocities $v_t = 1, 2, 3$ km/s. The sensitivity of the spectral region to changes in model parameters is shown in Fig. 4. It can be seen that temperature has a relatively larger effect on the depth of the CO features than metallicity and gravity. In this regard, a temperature change of 200 K is roughly equivalent to a change in metallicity of 1 dex or a change in gravity of Δlog $g = 1$.

The instrumental broadening was modelled by triangular profiles set to the resolution of the observed spectra. To find the best fits to observed spectra we follow the scheme of Jones et al. (2002). Namely, for every spectrum we carry out the minimisation of a 3D function $S = f(x_s, x_f, x_w) = 1/N \times \sum (1 - F_{obs}/F_{synt})^2$, where F_{obs}, F_{synt} are observed and computed fluxes, N is the number of points in the observed spectrum to be fitted, and $x_s, x_f,$ and x_w are relative shifts in wavelength scale, flux normalisation factor, and instrumental + rotational broadening, respectively. Rotational broadening was computed following Gray (1992). Figure 5 shows the sensitivity of our fit for GJ752B to the various model parameters. Figure 6 shows the observed and synthetic spectra fit for each object.

4 SPECTROSCOPIC ANALYSIS

The effective temperatures given in Table 1 were derived from averaging the temperatures derived by Dahn et al. (2002) and Vrba et al. (2004) across each spectral type and neglecting very young objects from the determination. For example a much lower effective temperature is derived for LP944-21, however, there is strong evidence (e.g. Ribas 2003) that the age of this object is < 0.5 Gyr rather than the 3 Gyr assumed by the methodology of Dahn et al. (2002) and Vrba et al. (2004). For early spectral types we use the effective temperature scales derived from Lane et al. (2001) and Segransan et al. (2003). We note these are consistent with
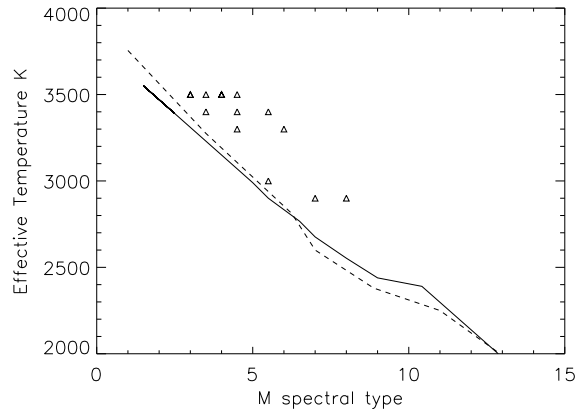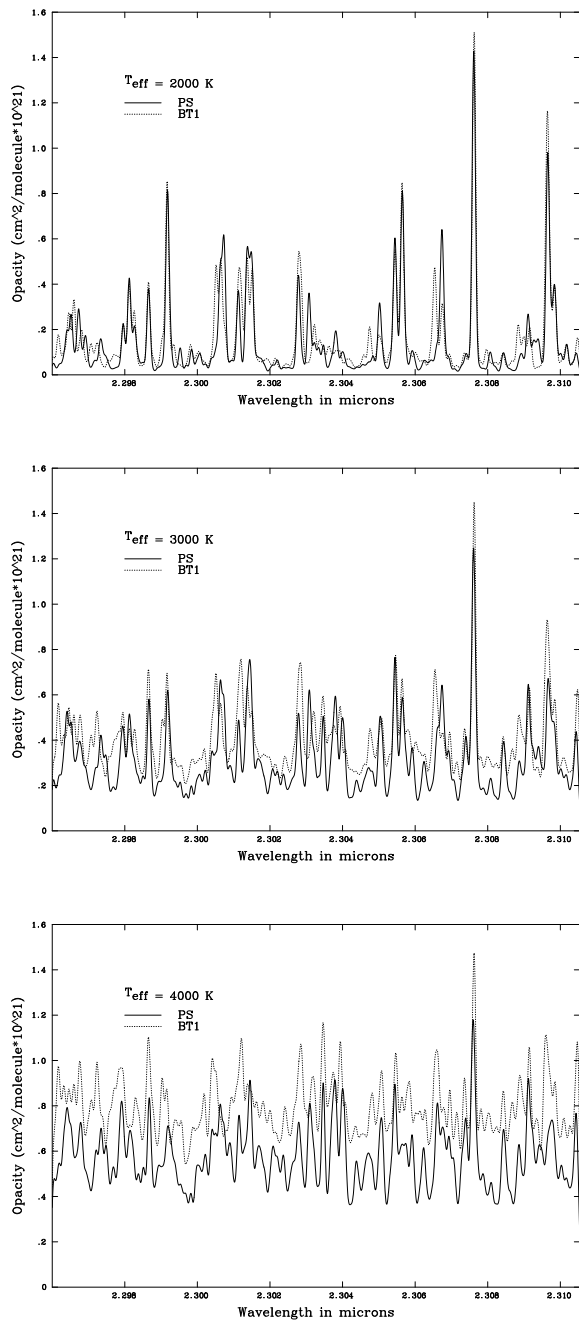

Figure 7. The triangles indicate best-fit temperatures for the observed sample given synthetic spectra where the metallicities are constrained to be solar and gravities constrained to be log g = 5.0. The solid line shows our adopted 'empirical' temperature scale, the dashed line shows a recent alternative scale from Golimowski et al. 2004.

detailed studies of GJ630.1A (Viti et al. 2002) and GJ699 (Dawson & de Robertis 2004). From here on we consider the effective temperatures in Table 1 as 'empirical' though this does assume that the radii of the evolutionary models that were used are accurate. Based on the comparisons of Chabrier & Baraffe (1995) this seems a reasonable working assumption.

In Table 2, we present best fit parameters determined using our minimisation technique on our observational spectra of sources with spectral types $\leq$M8. As suggested by the work of Mohanty & Basri (2003) and Bailer-Jones (2004), it appears that our rotational velocities show a general increase toward later spectral types. Although with the modest sample size presented here we are not in a position to further advance this area of work. Nonetheless, it should be noted that the density of strong CO features makes this an efficient region in which to derive rotational velocities and radial velocities. In addition to so-called 'unconstrained fits' where minimisation takes into account all parameters, we also give two cases of 'constrained fits'. In the first constrained fit we set [M/H]=0 and fit T_{eff} and log g, and in the second constrained fit we set T_{eff} equal to the empirical T_{eff} and fit log g and [M/H].

Our unconstrained minimisation solutions suggest temperatures higher than would be expected from the empirical temperatures of the objects. Relatively high temperatures are also found for the [M/H]=0 constrained fit. Our empirical T_{eff} constrained fit indicates a tendency to improbably low metallicities for almost all of the sample. We consider this discrepancy to arise from the fact that CO bands become weaker for decreasing metallicity or increasing temperature in a similar manner. Thus, if the models want to fit a higher T_{eff}, but are forced to fit a lower one, then they will fit a lower [M/H] to compensate.

In Fig. 7 we plot empirical and derived temperature scales against one another. It can be seen that for almost all objects our 'derived' effective temperatures (triangles) are higher than expected for empirical temperatures. Given
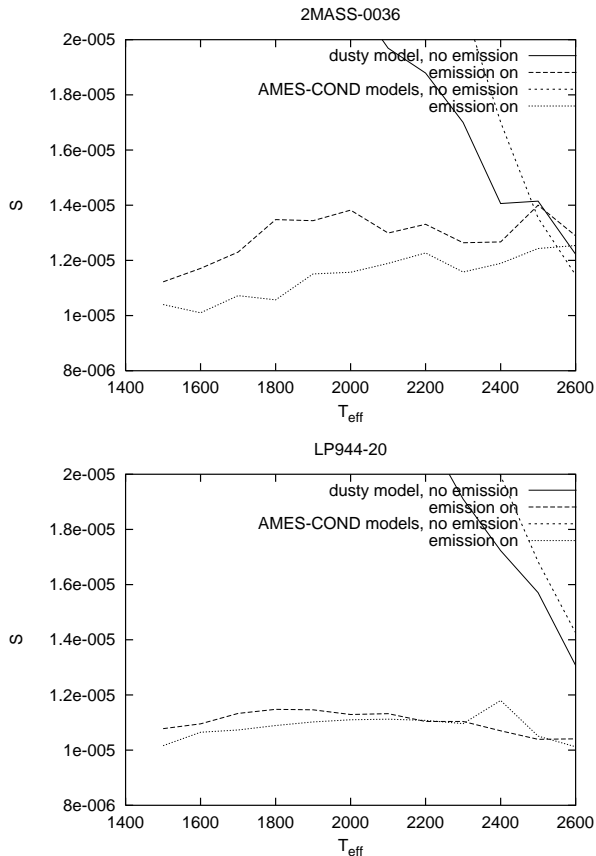
Figure 8. Water vapour opacity for different water vapour line lists, the solid line shows the Partridge & Schwenke 1997 (PS) list and the dotted line the Barber & Tennyson 2004 (BT1) list. While across the chosen wavelength region they are spectroscopically similar the overall opacity is rather different.

the good match of synthetic to observed spectral features one might expect more similar empirical and synthetic temperature scales. Such a discrepancy between empirical and synthetic temperature scale is a long standing result which has been arrived at by a number of routes: from fits to (1) the overall spectral energy distribution (e.g., Berriman & Reid 1987), (2) atomic lines (e.g., Jones et al. 1996), (3) wa-

ter vapour (Jones et al. 2002), (4) carbon monoxide (e.g., Pavlenko & Jones 2002). However, the temperature discrepancy for low-mass stars is usually discussed for stars with T_{eff} <3000 K, and is generally taken to be an effect arising from the inability of models to accurately treat dust formation (e.g. Dahn et al. 2002). We find the temperature discrepancy for apparently well-modelled spectra to be prevalent up to at least 3500 K. On the premise that the 'empirical' temperature scales are closer to reality, the offset suggests that the model structures are too hot for a given effective temperature. For GJ752B we have experimented with altering the model temperature structure. We find that substantial structural changes are necessary to adjust synthetic temperatures by the few hundred K needed to fit empirical ones. Since temperature discrepancies of 200 K translate into uncertainties of 1 dex in [M/H] or $\Delta \log g$=1 it is not possible to have confidence in our minimisation values for these properties. The temperature offset for the cooler objects such as GJ752B (T_{eff}=2550K) might be explained by the presence of relatively poorly quantified dust opacities. However, since the offset is also apparent above 3000 K where dust will not form (e.g., Tsuji 2002) it seems likely that at least part of the temperature scale problem is not due to dust. Instead we consider that the temperature scale problem may arise from a lack of high temperature water opacities.

As expected from our previous high resolution CO work (Viti et al. 2002), our current fits of the synthetic to observational spectra are encouraging. This is primarily due to our choice of a spectral region dominated by a well understood absorber (CO). However, it is clear from Figure 3 that water vapour opacity also plays a role in this spectral region. While the Partridge & Schwenke (1997) water vapour line list is clearly excellent at long wavelengths (Jones et al. 2002), there are significant discrepancies around 1.6 and 2.2 μm (Allard, Hauschildt & Schwenke 2000) and most probably around 0.95 μm as well.

In Fig. 8 we compare the Partridge & Schwenke (1997) water vapour line lists with the preliminary line list of Barber & Tennyson (2004, in preparation). The current version of the Barber & Tennyson list (known as BT1) is fully converged and complete to J=50 and includes around 650 million transitions. The Partridge & Schwenke list is also complete in respect to J levels (it reaches J=55) and consists of around 308 million transitions. The PS list is cut off at approximately 28000 cm^{-1} (approximately as there is not a consistent cut-off level), whereas the BT1 list has a cut-off of 30000 cm^{-1}. Moreover, even at energies below 28,000 cm^{-1} many lines are missing in the PS list (probably due to lack of convergence, resulting in the omission of higher levels). BT1 uses a newer potential surface (Shirin et al. 2003) and better describes high temperature water vapour transitions. Figure 8 indicates that at 2000 K the line lists give rather similar results, though by 4000 K BT1 shows approximately a 25% increase in opacity. Spectroscopically the line lists are reasonably similar though substantial differences can be seen by 4000 K. It is clear that the extra opacity of BT1 arising from higher J levels and improved completeness will lead to a significant back-warming effect on the model atmosphere moving the photosphere outward and the effective temperature downward. We checked for spectral differences between BT1 and PS, however, they are relatively small and make no difference to our derived minimisation values. To see the

Figure 9. The minimisation values for the L dwarfs 2MASS-0036 and LP944 deduced using dusty and non-dusty model atmospheres with and without emission. Minimisation values have been derived across the relevant model grid of temperatures though log g has been fixed at 5.0 and [M/H] has been fixed at the solar value.

effect of the increased opacity on the atmospheric structure of cool dwarfs it will be necessary to compute a new grid of model atmospheres. This will begin once the process of checking BT1 is complete, for example, by assigning quantum numbers to the transitions of lines in the laboratory emission spectrum of water at 3200 K (Coheur et al. 2004).

4.1 Below 2500 K – LP944 and 2MASS0036

Below 2500 K we do not easily find a satisfactory minimisation solution for the M9 dwarf LP944-20 and the L4 dwarf 2M0036, using any of the grids of model atmospheres (NextGen, AMES-Cond and Dusty). The results of our experiments are shown in Figure 9. The dusty and non-dusty models (solid and short dashed lines respectively) both suggest best fit temperatures higher than the edge of the model grid (> 2600 K). While such temperatures might possibly be plausible for LP944-20, the 'empirical' temperature for 2MASS0036 is a mere 1900 K. While incomplete water vapour may be crucial at higher temperature, the relative similarity of the Partridge & Schwenke and Barber & Tennyson line lists around 2000 K means that water vapour opacity is unlikely to be the source of this discrepancy. The discrepancy is probably more likely to arise from an inappro-

priate treatment of dust opacity. While a more sophisticated dust model is certainly appropriate (e.g. Tsuji, Nakajima & Yanagisawa 2004) we also experiment with another possibility. Following the methodology of Pavlenko et al. (2004) we imagine that the 2.3 micron region is veiled by additional grey continuum absorption. The long-dashed and dotted lines in Figure 9 indicate that veiling serves to improve the minimisation values obtained and appealingly decreases the sensitivity of the model fit. While we have not considered whether the atmospheric conditions are conducive to dust emission it is interesting that such veiling could result in spectra where CO bands do not change in strength appreciably throughout the L spectral class (Reid et al. 2001, Geballe et al. 2002, Nakajima, Tsuji & Yanagisawa 2004). Overall, the flat nature of the minimisation values for "emission on" models and minimistations beyond the model grid for "emission off" models suggest that we are not in a position to constrain effective temperature for the coolest targets in our sample.

In order to resolve these issues the first priority must be to incorporate a new water vapour line list in model atmosphere calculations. From an observational viewpoint it is important to obtain high resolution spectra of appropriate molecular and atomic features at widely separated wavelengths. Such observations should enable us to distinguish the importance of dust at different wavelengths. Dust absorption affects not only the synthetic spectra but the structure of the atmosphere. The problem needs to be solved with a self-consistent approach which includes among other things: depletion of molecular species into dust particles, the structure of dust clouds and a reliable size and composition distribution. Consideration of these issues is planned for future models and papers.

5   CONCLUSIONS

Based on a comparison of high resolution synthetic and observed spectra in the near infrared region, we derive rotational velocities, temperatures, metallicities and gravities for a sample of well studied objects. While our spectra are well modelled and dominated by CO absorption bands we find temperatures that are higher than those found by more empirical methods from 2500-3500 K. The discrepancy at higher temperatures is particularly interesting, and we consider it to be indicative of missing opacity, probably due to hot water vapour transitions not currently included in model atmospheres. Below T_{eff}=2500K, the additional complication of dust formation is expected to be another factor that requires accurate modelling if we are to derive accurate parameters from spectral fits.

6   ACKNOWLEDGMENTS

REFERENCES

Allard F., Hauschildt P.H., Schwenke D, 2000, ApJ, 540, 1005

Allard F., Hauschildt P.H., Alexander D.R., Tamanai A., Schweitzer A., 2001, ApJ, 556, 357

Bailer-Jones C.A.L., 2004, A&A, 419, 703

Berriman G., Reid N., 1987, 227, 315

Carbon D. F., Milkey R. W., Heasley J. N., 1976, ApJ, 207, 253

Chabrier G., Baraffe I., 1995, ApJ, 451, 29

Coheur et al., 2005, J. Chem Phys, in press

Cushing M. C., Rayner J. R., Davis S. P., Vacca W. D., 2003, ApJ, 582, 1066

Dahn et al. 2002, AJ, 1124, 1170

Dawson P.C., de Robertis M.M., 2004, AJ, 127, 2909

Geballe T.R. et al., 2002, ApJ, 564, 466

Gizis J.E., 2002, ApJ, 575, 484

Golimowski, D. A, et al. 2004, astroph/2475

Goorvitch D., 1994, ApJS, 95, 535

Gray D.F., 1992, The observation and analysis of stellar photospheres, 2nd edn, Cambridge University Press

Gurvitz L.V., Weitz I.V., Medvedev V.A., 1982, Thermodynamic properties of individual substances, Moscow Science

Hauschildt P. H., Allard F., Baron E., 1999, ApJ, 512, 377

Jones H. R. A., Longmore A.. J., Allard F., Hauschildt P. H., 1996, NRAS, 280,77

Jones H.R.A., Pavlenko Y., Viti S., Tennyson J., 2002, MNRAS, 331, 871

Kirkpatrick J.D., Henry T., McCarthy D.W., 1991, ApJS, 77, 417

Kupka, F., Piskunov, N., Ryabchikova, T. A., Stempels, H. C., Weiss, W. W. 1999, A&AS, 138, 119.

Lane B.F., Zapatero M.R., Britton M.C., Martin E.L., Kulkarni S.R., 2001, ApJ, 560, 390

Leggett S. K., 1992, ApJS, 82, 351

Leggett S. K., Allard F., Hauschildt P H., 1998, ApJ, 509, 836L

Lyubchik Y, Jones H.R.A., Pavlenko Y. V., Viti S., Pickering J. C., Blackwell-Whitehead R., 2004, A&A, 416, 655

McGovern M.R., Kirkpatrick J.D., McLean I.S., Burgasser A.J., Prato L., Lowrance P.J., 2004, ApJ, 600, 1020

McLean I.S., McGovern M.R., Burgasser A.J., Kirkpatrick J.D., Prato L., Kim S.S., 2003, ApJ, 596, 561

Mohanty S., Basri G., 2003, ApJ, 583, 451

Nakajima T., Tsuji T., Yanagisawa K., 2004, ApJ, 607, 499

Partridge H., Schwenke D.J., 1997, J. Chem. Phys., 106, 4618

Pavlenko Y., 2000, Astron. Rep., 44, 219

Pavlenko Y., Geballe T.R., Evans A., Smalley B., Eyres S.P.S., Tyne V.H., Yakovina L.A., 2004, A&A, 417, L39

Pavlenko Y. & Jones H.R.A., 2002, A&A, 396, 967

Reid I.N., Burgasser A.J., Cruz K.L., Kirkpatrick J.D., Gizis J.E., 2001, ApJ, 121, 1710

Ribas I., 2003, A&A, 400, 279

Segransan D., Kervella P., Forveille T., Queloz D., 2003, A&A, 397, 5

Shirin S.V., Polyansky O.L., Zobov N.F., Barletta P., Tennyson J., 2003, J. Chem. Phys. 118, 2124

Tsuji T., 1973, 23, 411

Tsuji T., 2002, ApJ, 575, 264

Tsuji T., Nakajima T., Yanagisawa K., 2004, ApJ, 607, 511

Unsold, A., 1955 Physik der Sternatmospheren, 2nd ed. Springer. Berlin.

Vidler M., Tennyson J., 2000, J. Chem. Phys., 113, 9766

Viti S., Jones H. R. A., Maxted P., Tennyson J., 2002, MNRAS, 329, 290

Vrba F.J. et al. 2004, astroph/2272

Carbon Monoxide in low-mass dwarf stars

Hugh R. A. Jones[1,2], Yakiv Pavlenko[3], Serena Viti[4], R.J. Barber[4], Larisa A. Yakovina[3], David Pinfield[1], Jonathan Tennyson[4]

[1] *Astrophysics Research Institute, Liverpool John Moores University, Twelve Quays House, Egerton Wharf, Birkenhead CH41 1LD*

[2] *Centre for Astrophysics Research, University of Hertfordshire, College Lane, Hatfield, Hertfordshire AL10 9AB*

[3]*Main Astronomical Observatory of Academy of Sciences o Ukraine, Golosiiv woods, Kyiv-127, Ukraine 03680*

[4] *Department of Physics and Astronomy, University College London, Gower Street, London WC1E 6BT*

ABSTRACT

We compare high resolution infrared observations of the CO 3-1 bands in the 2.297–2.310 μm region of M dwarfs and one L dwarf with theoretical expectations. We find a good match between the observational and synthetic spectra throughout the 2000-3500K temperature regime investigated. Nonetheless, for the 2500-3500 K temperature range the temperatures that we derive from synthetic spectral fits are higher than expected from more empirical methods by several hundred K. In order to reconcile our findings with the empirical temperature scale it is necessary to invoke warming of the model atmosphere used to construct the synthetic spectra. We consider that the most likely reason for the back-warming is missing high temperature opacity. We compare the opacity of the Partridge & Schwenke (1997) line list used for the model atmosphere with the output from a preliminary calculation by Barber & Tennyson (2004). While the Partridge & Schwenke line list is a reasonable spectroscopic match for the new line list at 2000 K, by 4000 K it is missing around 25% of the water vapour opacity. We thus consider that the offset between empirical and synthetic temperature scales is explained by the lack of hot water vapour used for computation of the synthetic spectra. For our coolest objects with temperatures below 2500 K we find best fits when using synthetic spectra which include dust emission. Our spectra also allow us to constrain the rotational velocities of our sources, and these velocities are consistent with the broad trend of rotational velocities increasing from M to L.

1   INTRODUCTION

Low mass dwarf stars dominate our Galaxy in terms of number. They provide a probe of our understanding of main sequence stellar evolution and are the key in determining the boundary between stellar and sub-stellar objects. There are relatively few observations of known-mass low mass stars. Parameters such as effective temperature and metallicity, vital in determining positions in H-R diagrams, remain controversial. To reliably constrain the low-mass initial stellar mass function it is essential to know the basic properties of standard low-mass M, L and T dwarfs. A correct determination of the mass function relies on an accurate transformation from luminosity and temperature to mass. These relationships are sensitive to the stellar chemical composition. For hotter objects colour-colour diagrams are reasonably reliable indicators of temperature and metallicity. However such diagrams for low mass dwarfs do not yet reproduce the broadband fluxes within a reasonable error and therefore cannot be uniquely used to determine reliable temperatures, metallicities and gravities. Ideally it would be useful to have spectroscopic signatures sensitive to temperature, metallicity and gravity that are reproducible with synthetic spectra.

Many authors have determined the properties of low-mass objects using synthetic spectra. However, the use of such synthetic spectra are problematic because (1) the objects are dominated by various diatomic and triatomic molecules whose high temperature properties are poorly understood and (2) the large number of different transitions means that most transitions are substantially blended with other competing opacities. One potential route to resolve these issues is to try to find spectral regions where these issues are less problematic. For example the middle of the J-band window is a promising region (Jones et al. 1996; McLean et al. 2003). Although this region is relatively transparent and is in a wavelength regime where infrared spectrometers are relatively sensitive it does have shortcomings. In addition to the problems with modelling water vapour at short wavelengths (Jones et al. 2002), it is now clear that the poorly modelled opacities of FeH (Cushing et al. 2003), as well as VO and TiO (McGovern et al. 2004) also play an important role in this region.

Here we investigate an alternative wavelength regime. In the spectral region between 2.29 and 2.45 μm, CO is a key opacity for low mass stars. CO appears in a relatively easily-
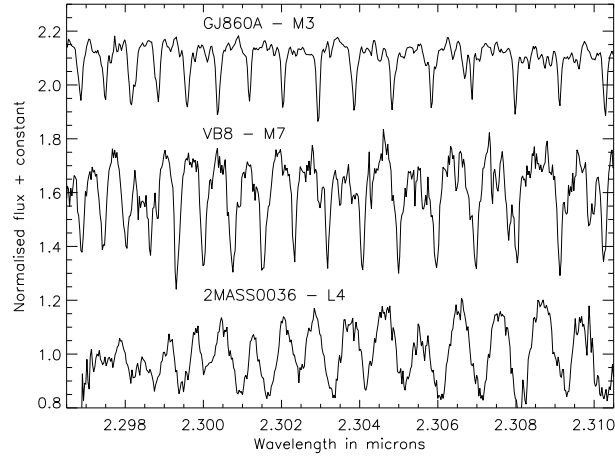
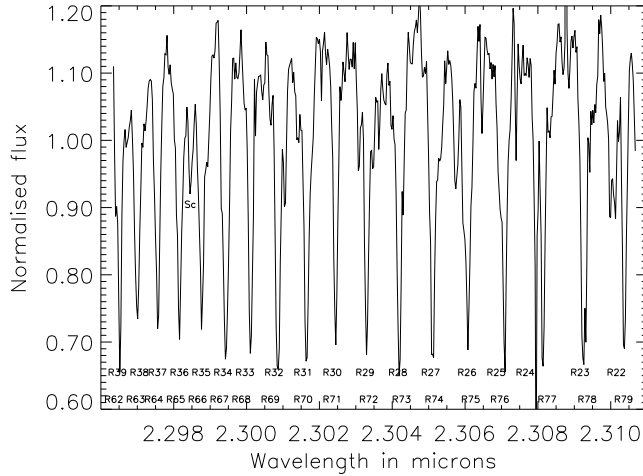**Figure 1.** Spectral sequence of CO bands from M3 to L4.

Figure 2. CO 3-1 transitions and Sc line identified in GJ752B. The resolution of the data is insufficient to unambiguously identify the higher energy (R62 to R79).

observed stable part of the K band and molecular data, including f-values, are well known. Moreover, CO is believed to be formed under LTE (e.g. Carbon et al. 1976) and therefore the levels are populated according to the Boltzmann distribution. The available CO line list has proven to be reliable for solar work and so is believed to be more than adequate for the lower energy states accessed in cool dwarf atmospheres (Goorvitch 1994). The other significant metal diatomic species appearing in infrared cool dwarf stars are FeH, VO and TiO, however, these diatomics are not as prominent as CO and at the time the observations were taken for this paper no adequate line lists existed for these species.

In Pavlenko & Jones (2002) we showed that the $\Delta\nu$=2 carbon monoxide bands around 2.3–2.4 μm can be well modelled by synthetic spectra. This region is dominated by CO and
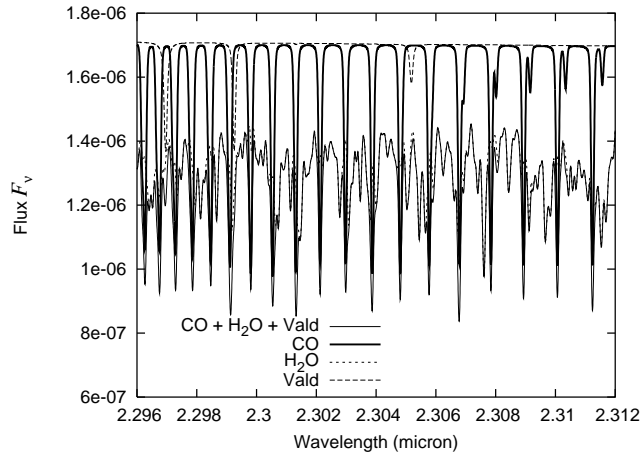
Figure 3. The plot shows the various opacity contributions for a 3000 K log g=5.0 solar metallicity model from atomic lines (top of plot, dashed line), carbon monoxide transitions (top of the plot, thick solid line), water vapour (dotted line) and the overall formation of the continuum primarily dominated by water (thin solid line).
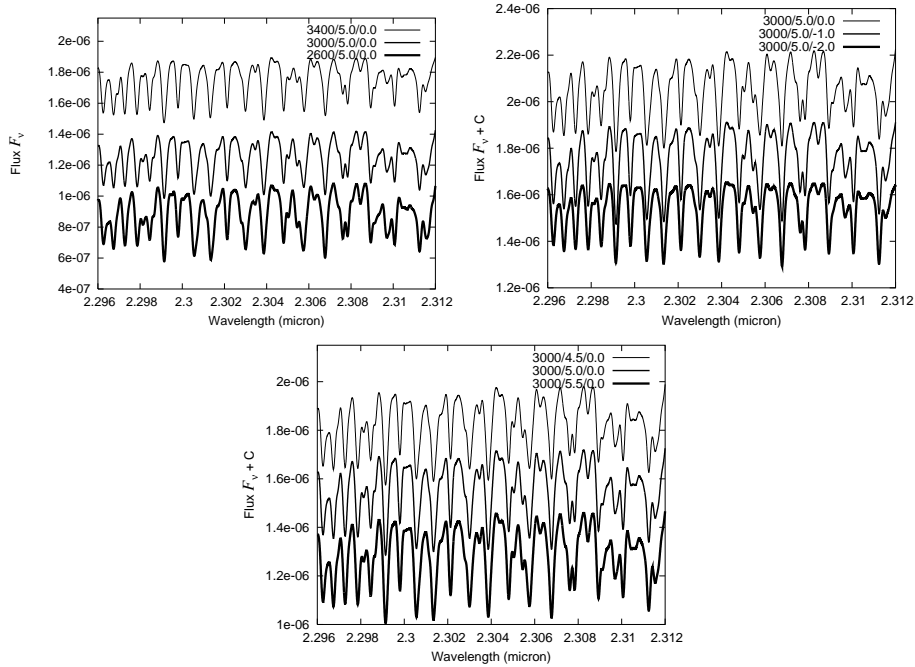
Figure 4. The above plots show the temperature, metallicity and gravity dependence of synthetic spectra around a base model of 3000 K, solar metallicity, log g = 5.0. The spectra have been offset for clarity.

H_2O bands, and has few atomic lines of significance. This is advantageous because CO is well modelled relative to the current quality of atomic oscillator strengths in the infrared (e.g. Jones et al. 1996, Lyubchik et al. 2004). Here we extend this work to much higher resolution, where the CO bands are very distinct from the water vapour modelled continuum. The wavelength range (2.297 to 2.311 microns) was chosen on the basis of features in late type dwarf spectra identified to be relatively metallicity sensitive and reproducible by synthetic spectra in Viti et al. (2002).

Table 1. Literature properties of observed targets: kinematic classification (KIN-class) are from Leggett (1992) and Leggett et al. (1998), spectral types are from Kirkpatrick, Henry & McCarthy (1991) and Gizis (2002) and empirical temperatures derived using Lane et al. (2001), Segransan et al. (2003), Dahn et al. (2002) and Vrba et al. (2004).

Object	KIN-class	Sp Type	Empirical temperature (K)
GJ860A	OD	dM3	3310
GJ725A	OD	dM3	3310
GJ725B	OD	dM3.5	3230
GJ896A	YD	dM3.5	3230
G87-9B	–	dM4	3150
GJ699	O/H	dM4	3150
GJ860B	OD	dM4	3150
GJ896B	YD	dM4.5	3070
GJ630.1A	H	dM4.5	3070
GJ166C	OD	dM4.5	3070
GJ2005ABCD	OD	dM5.5	2910
GJ65A	YD	dM5.5	2910
GJ65B	YD	dM6	2825
GJ644C	OD	dM7	2670
GJ752B	OD	dM8	2550
LP944-20	YD	dM9	2440
2MASS0036	-	dL4	1900

Table 2. Derived synthetic spectra parameters are given. The syntax for the models is T_{eff} / log g / [M/H] so for example 2800/6.0/-0.5 means a 2800 K, gravity = 6.0 cm/s and metallicity –0.5 dex model. Rotational velocities are derived from the unconstrained minimisation fit and are typically accurate to 3 km/s. Values given in italic are fixed. The values for the minimisation of coolest objects LP944-20 and 2MASS0036 (shortened its full designation of 2MASS J00361617+1821104) are rather dependent on the details of the model. Minimisations for these objects are presented in Fig. 9.

Object	Rotational velocity v sin i (km/s)	unconstrained minimisation	[M/H] constrained T_{eff} & log g minimisation	T_{eff} constrained [M/H] & log g minimisation
GJ860A	7.0	3500/5.5/0.0	35/5.5/*0.0*	*3300*/5.0/-1.0
GJ725A	5.0	3500/5.5/-0.5	36/5.5/*0.0*	*3300*/5.0/-1.5
GJ725B	7.0	3500/5.5/0.0	35/5.5/*0.0*	*3200*/5.0/-1.5
GJ896A	10.0	3400/4.5/-1.5	36/5.5/*0.0*	*3200*/4.5/-2.0
G87-9B	6.0	3500/4.5/-0.5	35/5.5/*0.0*	*3200*/5.0/-1.5
GJ699	5.0	3500/4.5/-0.5	36/5.5/*0.0*	*3200*/4.5/-2.0
GJ860B	8.0	3500/5.5/0.0	35/5.5/*0.0*	*3200*/4.5/-1.5
GJ896B	15.0	3500/5.0/-0.5	35/5.5/*0.0*	*3100*/4.5/-2.0
GJ630.1A	27.5	3300/5.0/-0.5	33/5.0/*0.0*	*3100*/4.5/0.0
GJ166C	5.0	3400/5.5/-0.5	35/5.5/*0.0*	*3000*/4.5/-2.0
GJ2005ABCD	14.0	3000/5.5/-1.0	33/4.5/*0.0*	*2900*/5.0/-1.5
GJ65A	31.5	3400/4.5/0.0	34/4.5/*0.0*	*2900*/5.5/-1.5
GJ65B	29.5	3300/4.5/0.0	33/4.5/*0.0*	*2800*/5.5/-1.5
GJ644C	12.5	2900/4.5/0.0	29/4.5/*0.0*	*2700*/5.0/-1.0
GJ752B	10.5	2900/5.5/0.0	29/5.5/*0.0*	*2600*/5.0/-1.5
LP944-30	31.0	–	–	–
2MASS0036	38.0	–	–	–

2   OBSERVATIONS

The targets chosen for this study are all bright relatively well-studied M and L dwarfs. The source selection was made in order to give good coverage in spectral type and metallicity. However, the half nights available to us limited our sample to a relatively restricted range of right ascension. The sample is shown in Table 1.

The targets were observed during the first half of the nights of 2001 September 8–12 with the Cooled Grating Spectrometer 4 (CGS4) on the UK Infrared Telescope (UKIRT)

on Mauna Kea, Hawaii. The weather was photometric throughout with optical seeing of typically 0.8". Comparison sky spectra were obtained by nodding the telescope so that the object was measured successively in two rows of the array, separated by 30 arcsec.

The echelle grating in 24th order at a central wavelength setting of 2.304 microns was used for all observations. This setup gives wavelength coverage from 2.297 to 2.311 microns at a resolution of approximately 42000.

To remove telluric bands of water, oxygen, carbon dioxide and methane, we observed A and B standard stars. Such stars are not expected to have features in common with cool dwarf stars and appear to be featureless across our spectral range. Wavelength calibration was carried out using a xenon arc lamp. This generally worked well because although there are only four lines available in this region, the xenon lines at 2.29 and 2.31 microns fall at either edge of the array and so provide a good wavelength calibration. The only caveat to this is that the CVF positioning is only accurate to around 20 pixels and so the desired wavelength interval is sometimes shifted redward or blueward by around 0.001 microns. Our cross-correlation tests indicate that the wavelength calibration was better than 0.0001 microns. Sky subtraction was done with standard routines which take into account any residual sky emission due to variation of the sky brightness between paired object and sky spectra. The signal was spread between three rows. To extract the spectrum from the sky subtracted signal an Optimal Extraction technique was used; this combines the rows using weights based on the spatial profile of the stellar image. The spectra were reduced using the *Figaro*, *Specdre* and *Kappa* packages provided and supported by Starlink.

A spectral sequence from M3 to L4 is shown in Fig. 1. It can be seen from Figure 2 that individual rotational CO transitions can be resolved in our observed spectra. The CO opacities in our spectra are made up of a large number of spectral lines, covering a wide intensity range, of the second overtone ($\nu = 2\text{--}0$). The second overtone band of CO originates from vibration-rotation transitions in the ground electronic state $X^1\Sigma$ and obeys the selection rules $\Delta\nu = 2$ and $\Delta J = \pm 1$. The band head of the second overtone (i.e the point at which the separation between the R transitions is zero), occurs at ~ 2.290 μm and therefore both 'hot' (such as R77) and 'cold' (such as R24) rotational transitions are seen in our spectra.
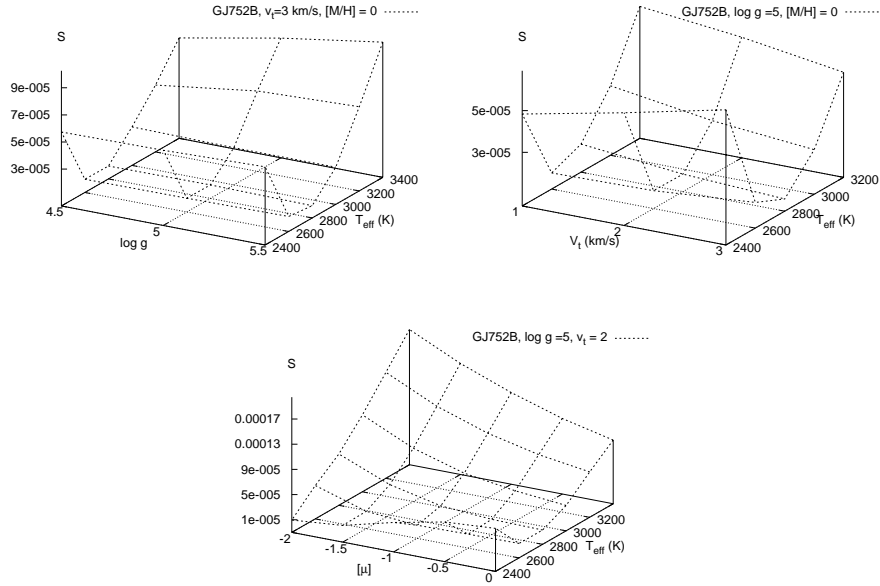
Figure 5. Surface plots showing the sensitivity of the best fit temperature of GJ752B to metallicity, gravity and turbulent velocity. A base model of solar metallicity, log g=5.0 and v_t=3km/s is used.

3 THE MODELS

Model atmospheres from the Phoenix code were used for this work. In particular we used the grid known as NextGen (Hauschildt et al. 1999) but also Dusty (Allard et al. 2001) and AMES-COND models (Allard et al. 2001). Model temperatures of 1500 to 3800 K, metallicities of [M/H]= -2.0 to 0.0 and gravities of log $g = 4.5$ to 5.5 are considered. These parameters represent the probable extremes for the sample based on the literature. We have not tried comparing the system with models computed with non-solar abundance patterns.

Computations of local thermal equilibrium synthetic spectra were carried out by the program WITA6 (Pavlenko 2000). This model assumes LTE, hydrostatic equilibrium for a one-dimensional model atmosphere, and no sources or sinks of energy. The equations of ionisation-dissociation equilibrium were solved for media consisting of atoms, ions and molecules. We took into account $\sim$ 100 components (Pavlenko 2000). The constants for equations of chemical balance were taken from Tsuji (1973). It is worth noting that the chemical balance in cool dwarf atmospheres is governed by the CO molecule (Pavlenko & Jones 2002).

The Partridge & Schwenke (1997: PS) line list is used as the primary source of water vapour lines, though we also made some comparisons with the preliminary line list of Barber & Tennyson (known as BT1, 2004). The partition functions of H_2O were also computed on
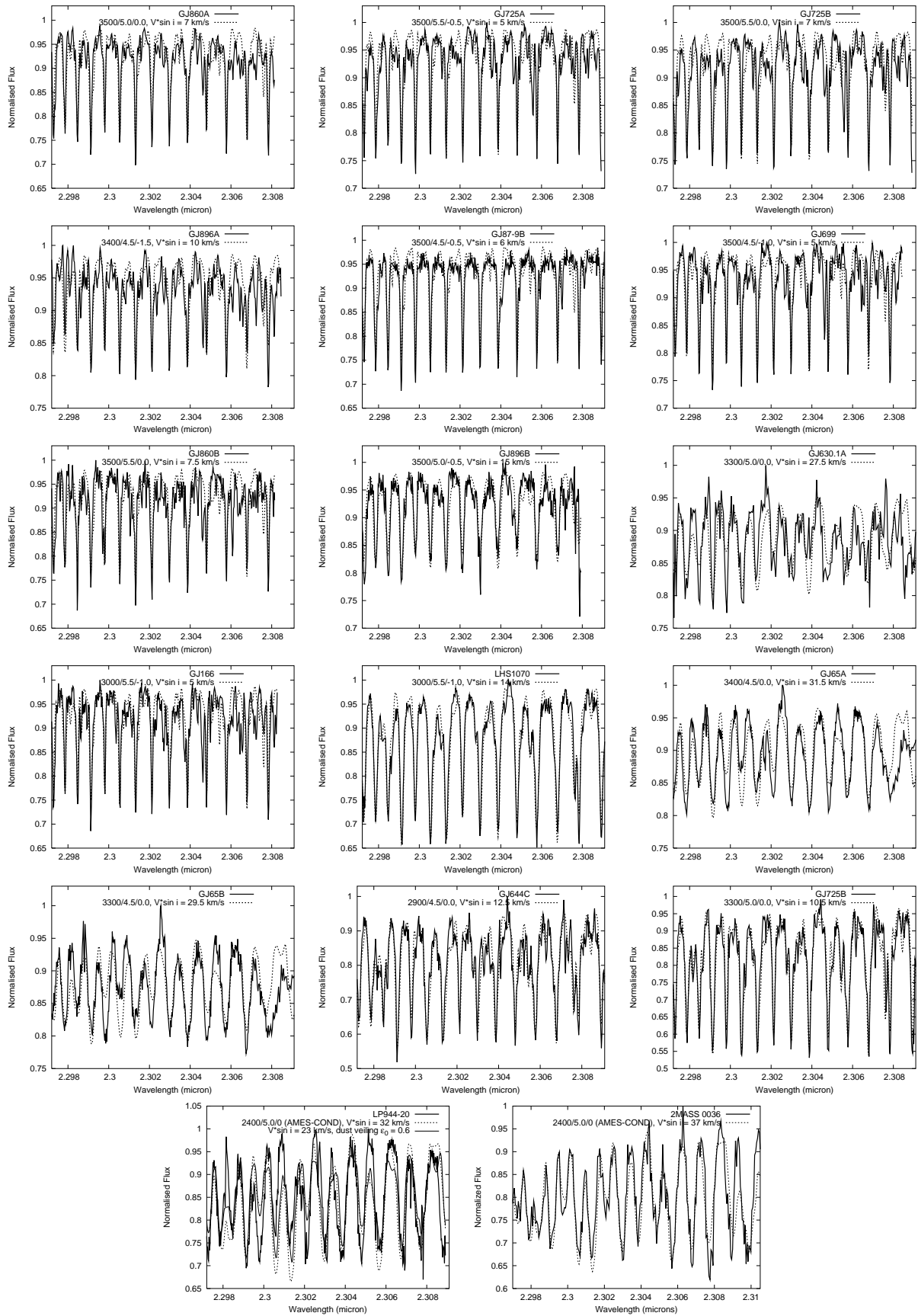
Figure 6. The observational data are overlaid with the best fit 'unconstrained' synthetic spectra except for LP944-20 and 2MASS0036 for which representative models are shown.
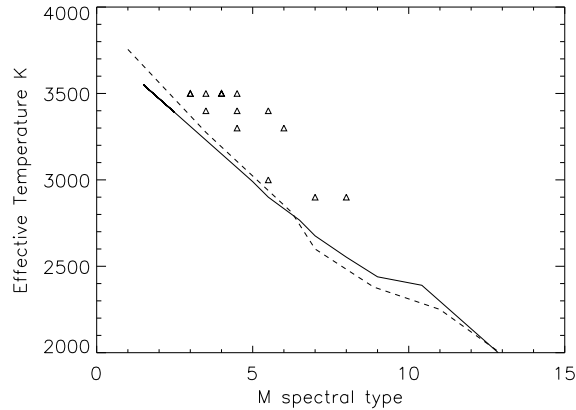
the PS line list following Pavlenko et al. (2004). We recomputed the constants of dissociation equilibrium using the H_2O partition function following Vidler & Tennyson (2000) though found no significant differences for test synthetic spectra at 3200 K, log $g = 5$ and 2400 K, log $g = 5$ (Pavlenko et al, 2004, in preparation). For CO, we used the $^{12}C^{16}O$ and $^{13}C^{16}O$ line lists of Goorvitch (1994). The CO partition functions were taken from Gurvitz, Weitz & Medvedev (1982). The atomic line list was taken from VALD (Kupka et al. 1999). The relative importance of the different opacities contributing to our synthetic spectra is shown in Fig. 3.

The profiles of molecular and atomic lines are determined using the Voigt function $H(a, v)$, parameters of their natural broadening C_2 and van der Waals broadening C_4 from databases (Kupka et al. 1999) or in their absence computed following Unsold (1955). Owing to the low temperatures in cool dwarf atmospheres, and consequent low electron densities, Stark broadening may be neglected. Computations for synthetic spectra were carried out with a 0.00005 μm step for microturbulent velocities $v_t = 1, 2, 3$ km/s. The sensitivity of the spectral region to changes in model parameters is shown in Fig. 4. It can be seen that temperature has a relatively larger effect on the depth of the CO features than metallicity and gravity. In this regard, a temperature change of 200 K is roughly equivalent to a change in metallicity of 1 dex or a change in gravity of Δlog $g = 1$.

The instrumental broadening was modelled by triangular profiles set to the resolution of the observed spectra. To find the best fits to observed spectra we follow the scheme of Jones et al. (2002). Namely, for every spectrum we carry out the minimisation of a 3D function $S = f(x_s, x_f, x_w) = 1/N \times \sum(1 - F_{obs}/F_{synt})^2$, where F_{obs}, F_{synt} are observed and computed fluxes, N is the number of points in the observed spectrum to be fitted, and x_s, x_f, and x_w are relative shifts in wavelength scale, flux normalisation factor, and instrumental + rotational broadening, respectively. Rotational broadening was computed following Gray (1992). Figure 5 shows the sensitivity of our fit for GJ752B to the various model parameters. Figure 6 shows the observed and synthetic spectra fit for each object.

4 SPECTROSCOPIC ANALYSIS

The effective temperatures given in Table 1 were derived from averaging the temperatures derived by Dahn et al. (2002) and Vrba et al. (2004) across each spectral type and neglecting very young objects from the determination. For example a much lower effective temperature
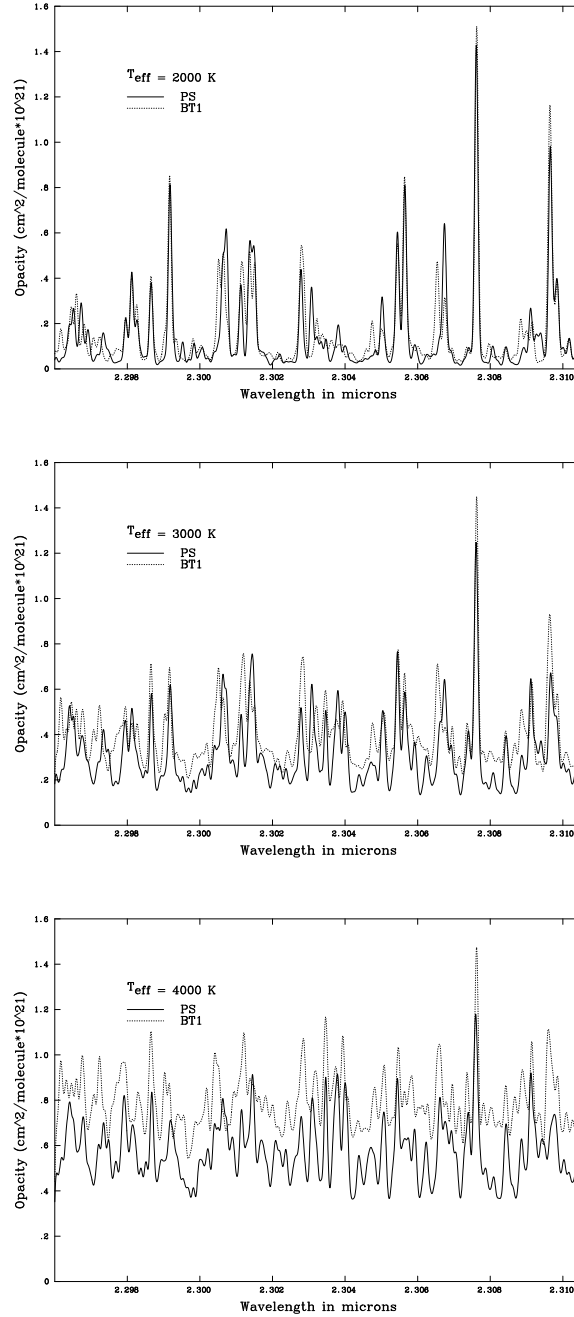
Figure 7. The triangles indicate best-fit temperatures for the observed sample given synthetic spectra where the metallicities are constrained to be solar and gravities constrained to be log g = 5.0. The solid line shows our adopted 'empirical' temperature scale, the dashed line shows a recent alternative scale from Golimowski et al. 2004.

is derived for LP944-21, however, there is strong evidence (e.g. Ribas 2003) that the age of this object is < 0.5 Gyr rather than the 3 Gyr assumed by the methodology of Dahn et al. (2002) and Vrba et al. (2004). For early spectral types we use the effective temperature scales derived from Lane et al. (2001) and Segransan et al. (2003). We note these are consistent with detailed studies of GJ630.1A (Viti et al. 2002) and GJ699 (Dawson & de Robertis 2004). From here on we consider the effective temperatures in Table 1 as 'empirical' though this does assume that the radii of the evolutionary models that were used are accurate. Based on the comparisons of Chabrier & Baraffe (1995) this seems a reasonable working assumption.

In Table 2, we present best fit parameters determined using our minimisation technique on our observational spectra of sources with spectral types $\leq$M8. As suggested by the work of Mohanty & Basri (2003) and Bailer-Jones (2004), it appears that our rotational velocities show a general increase toward later spectral types. Although with the modest sample size presented here we are not in a position to further advance this area of work. Nonetheless, it should be noted that the density of strong CO features makes this an efficient region in which to derive rotational velocities and radial velocities. In addition to so-called 'unconstrained fits' where minimisation takes into account all parameters, we also give two cases of 'constrained fits'. In the first constrained fit we set [M/H]=0 and fit T_{eff} and log g, and in the second constrained fit we set T_{eff} equal to the empirical T_{eff} and fit log g and [M/H].

Our unconstrained minimisation solutions suggest temperatures higher than would be expected from the empirical temperatures of the objects. Relatively high temperatures are
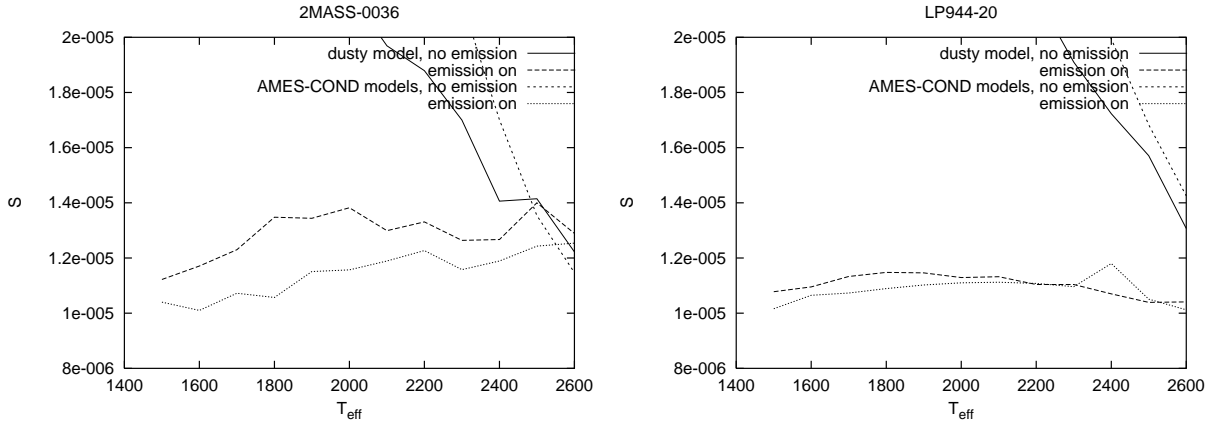
Figure 8. Water vapour opacity for different water vapour line lists, the solid line shows the Partridge & Schwenke 1997 (PS) list and the dotted line the Barber & Tennyson 2004 (BT1) list. While across the chosen wavelength region they are spectroscopically similar the overall opacity is rather different.

also found for the [M/H]=0 constrained fit. Our empirical T_{eff} constrained fit indicates a tendency to improbably low metallicities for almost all of the sample. We consider this discrepancy to arise from the fact that CO bands become weaker for decreasing metallicity or increasing temperature in a similar manner. Thus, if the models want to fit a higher T_{eff}, but are forced to fit a lower one, then they will fit a lower [M/H] to compensate.

In Fig. 7 we plot empirical and derived temperature scales against one another. It can be seen that for almost all objects our 'derived' effective temperatures (triangles) are higher than expected for empirical temperatures. Given the good match of synthetic to observed spectral features one might expect more similar empirical and synthetic temperature scales. Such a discrepancy between empirical and synthetic temperature scale is a long standing result which has been arrived at by a number of routes: from fits to (1) the overall spectral energy distribution (e.g., Berriman & Reid 1987), (2) atomic lines (e.g., Jones et al. 1996), (3) water vapour (Jones et al. 2002), (4) carbon monoxide (e.g., Pavlenko & Jones 2002). However, the temperature discrepancy for low-mass stars is usually discussed for stars with T_{eff} <3000 K, and is generally taken to be an effect arising from the inability of models to accurately treat dust formation (e.g. Dahn et al. 2002). We find the temperature discrepancy for apparently well-modelled spectra to be prevalent up to at least 3500 K. On the premise that the 'empirical' temperature scales are closer to reality, the offset suggests that the model structures are too hot for a given effective temperature. For GJ752B we have experimented with altering the model temperature structure. We find that substantial structural changes are necessary to adjust synthetic temperatures by the few hundred K needed to fit empirical ones. Since temperature discrepancies of 200 K translate into uncertainties of 1 dex in [M/H] or $\Delta \log g$=1 it is not possible to have confidence in our minimisation values for these properties. The temperature offset for the cooler objects such as GJ752B (T_{eff}=2550K) might be explained by the presence of relatively poorly quantified dust opacities. However, since the offset is also apparent above 3000 K where dust will not form (e.g., Tsuji 2002) it seems likely that at least part of the temperature scale problem is not due to dust. Instead we consider that the temperature scale problem may arise from a lack of high temperature water opacities.

As expected from our previous high resolution CO work (Viti et al. 2002), our current fits of the synthetic to observational spectra are encouraging. This is primarily due to our choice of a spectral region dominated by a well understood absorber (CO). However, it is clear from Figure 3 that water vapour opacity also plays a role in this spectral region. While the Partridge & Schwenke (1997) water vapour line list is clearly excellent at long wavelengths (Jones et al. 2002), there are significant discrepancies around 1.6 and 2.2 μm (Allard, Hauschildt & Schwenke 2000) and most probably around 0.95 μm as well.

In Fig. 8 we compare the Partridge & Schwenke (1997) water vapour line lists with the preliminary line-list of Barber & Tennyson (2004, in preparation). The current version of

Figure 9. The minimisation values for the L dwarfs 2MASS-0036 and LP944 deduced using dusty and non-dusty model atmospheres with and without emission.

the Barber & Tennyson list (known as BT1) is fully converged and complete to J=50 and includes around 650 million transitions. The Partridge & Schwenke list is also complete in respect to J levels but consists of around 308 million transitions. As well as using a newer potential surface (Shirin et al. 2003), the full convergence and higher J limit of BT1 means that it better describes high temperature water vapour transitions. The PS list is cut off at approximately 28000 cm^{-1} (approximately as there is not a consistent cut-off level), whereas the BT1 list has a cut-off of 30000 cm^{-1}. Moreover, even at energies below 28,000 cm^{-1} many lines are missing in the PS list (probably due to lack of convergence, resulting in the omission of higher levels). Figure 8 indicates that at 2000 K the line lists give rather similar results, though by 4000 K BT1 shows approximately a 25% increase in opacity. Spectroscopically the line lists are reasonably similar though substantial differences can be seen by 4000 K. It is clear that the extra opacity of BT1 arising from higher J levels and improved completeness will lead to a significant back-warming effect on the model atmosphere moving the photosphere outward and the effective temperature downward. We checked for spectral differences between BT1 and PS, however, they are relatively small and make no difference to our derived minimisation values. To see the effect of the increased opacity on the atmospheric structure of cool dwarfs it will be necessary to compute a new grid of model atmospheres. This will begin once the process of checking BT1 is complete, for example, by assigning quantum numbers to the transitions of lines in the laboratory emission spectrum of water at 3200 K (Coheur et al. 2004, in preparation).

4.1   Below 2500 K – LP944 and 2MASS0036

Below 2500 K we do not easily find a satisfactory minimisation solution for the M9 dwarf LP944-20 and the L4 dwarf 2M0033, using any of the grids of model atmospheres (NextGen, AMES-Cond and Dusty). The results of our experiments are shown in Figure 9. The dusty and non-dusty models (solid and short dashed lines respectively) both suggest best fit temperatures higher than the edge of the model grid (> 2600 K). While such temperatures might possibly be plausible for LP944-20, the 'empirical' temperature for 2MASS0036 is a mere 1900 K. While incomplete water vapour may be crucial at higher temperature, the relative similarity of the Partridge & Schwenke and Barber & Tennyson line lists around 2000 K means that water vapour opacity is unlikely to be the source of this discrepancy. The discrepancy is probably more likely to arise from an inappropriate treatment of dust opacity. While a more sophisticated dust model is certainly appropriate (e.g. Tsuji, Nakajima & Yanagisawa 2004) we also experiment with another possibility. Following the methodology of Pavlenko et al. (2004) we imagine that the 2.3 micron region is veiled by additional grey continuum absorption. The long-dashed and dotted lines in Figure 9 indicate that veiling serves to improve the minimisation values obtained and appealingly decreases the sensitivity of the model fit. While we have not considered whether the atmospheric conditions are conducive to dust emission it is interesting that such veiling could result in spectra where CO bands do not change in strength appreciably throughout the L spectral class (Reid et al. 2001, Geballe et al. 2002, Nakajima, Tsuji & Yanagisawa 2004). Nonetheless the values obtained still suggest best fits beyond the edge of the model grid.

In order to resolve these issues the first priority must be to incorporate a new water vapour line list in model atmosphere calculations. From an observational viewpoint it is important to obtain high resolution spectra of appropriate molecular and atomic features at widely separated wavelengths. Such observations should enable us to distinguish the importance of dust at different wavelengths. Dust absorption affects not only the synthetic spectra but the structure of the atmosphere. The problem needs to be solved with a self-consistent approach which includes among other things: depletion of molecular species into dust particles, the structure of dust clouds and a reliable size and composition distribution. Consideration of these issues is planned for future models and papers.

5 CONCLUSIONS

Based on a comparison of high resolution synthetic and observed spectra in the near infrared region, we derive rotational velocities, temperatures, metallicities and gravities for a sample of well studied objects. While our spectra are well modelled and dominated by CO absorption bands we find temperatures that are higher than those found by more empirical methods from 2500-3500 K. The discrepancy at higher temperatures is particularly interesting, and we consider it to be indicative of missing opacity, probably due to hot water vapour transitions not currently included in model atmospheres. Below T_{eff}=2500K, the additional complication of dust formation is expected to be another factor that requires accurate modelling if we are to derive accurate parameters from spectral fits.

6 ACKNOWLEDGMENTS

REFERENCES

Allard F., Hauschildt P.H., Schwenke D, 2000, ApJ, 540, 1005

Allard F., Hauschildt P.H., Alexander D.R., Tamanai A., Schweitzer A., 2001, ApJ, 556, 357

Bailer-Jones C.A.L., 2004, A&A, 419, 703

Berriman G., Reid N., 1987, 227, 315

Carbon D. F., Milkey R. W., Heasley J. N., 1976, ApJ, 207, 253

Chabrier G., Baraffe I., 1995, ApJ, 451, 29

Cushing M. C., Rayner J. R., Davis S. P., Vacca W. D., 2003, ApJ, 582, 1066

Dahn et al. 2002, AJ, 1124, 1170

Dawson P.C., de Robertis M.M., 2004, AJ, 127, 2909

Geballe T.R. et al., 2002, ApJ, 564, 466

Gizis J.E., 2002, ApJ, 575, 484

Golimowski, D. A, et al. 2004, astroph/2475

Goorvitch D., 1994, ApJS, 95, 535

Gray D.F., 1992, The observation and analysis of stellar photospheres, 2nd edn, Cambridge University Press

Gurvitz L.V., Weitz I.V., Medvedev V.A., 1982, Thermodynamic properties of individual substances, Moscow Science

Hauschildt P. H., Allard F., Baron E., 1999, ApJ, 512, 377

Jones H. R. A., Longmore A.. J., Allard F., Hauschildt P. H., 1996, NRAS, 280,77

Jones H.R.A., Pavlenko Y., Viti S., Tennyson J., 2002, MNRAS, 331, 871

Kirkpatrick J.D., Henry T., McCarthy D.W., 1991, ApJS, 77, 417

Kupka, F., Piskunov, N., Ryabchikova, T. A., Stempels, H. C., Weiss, W. W. 1999, A&AS, 138, 119.

Lane B.F., Zapatero M.R., Britton M.C., Martin E.L., Kulkarni S.R., 2001, ApJ, 560, 390

Leggett S. K., 1992, ApJS, 82, 351

Leggett S. K., Allard F., Hauschildt P H., 1998, ApJ, 509, 836L

Lyubchik Y, Jones H.R.A., Pavlenko Y. V., Viti S., Pickering J. C., Blackwell-Whitehead R., 2004, A&A, 416, 655

McGovern M.R., Kirkpatrick J.D., McLean I.S., Burgasser A.J., Prato L., Lowrance P.J., 2004, ApJ, 600, 1020

McLean I.S., McGovern M.R., Burgasser A.J., Kirkpatrick J.D., Prato L., Kim S.S., 2003, ApJ, 596, 561

Mohanty S., Basri G., 2003, ApJ, 583, 451

Nakajima T., Tsuji T., Yanagisawa K., 2004, ApJ, 607, 499

Partridge H., Schwenke D.J., 1997, J. Chem. Phys., 106, 4618

Pavlenko Y., 2000, Astron. Rep., 44, 219

Pavlenko Y., Geballe T.R., Evans A., Smalley B., Eyres S.P.S., Tyne V.H., Yakovina L.A., 2004, A&A, 417, L39

Pavlenko Y. & Jones H.R.A., 2002, A&A, 396, 967

Reid I.N., Burgasser A.J., Cruz K.L., Kirkpatrick J.D., Gizis J.E., 2001, ApJ, 121, 1710

Ribas I., 2003, A&A, 400, 279

Segransan D., Kervella P., Forveille T., Queloz D., 2003, A&A, 397, 5

Shirin S.V., Polyansky O.L., Zobov N.F., Barletta P., Tennyson J., 2003, J. Chem. Phys. 118, 2124

Tsuji T., 1973, 23, 411

Tsuji T., 2002, ApJ, 575, 264

Tsuji T., Nakajima T., Yanagisawa K., 2004, ApJ, 607, 511

Unsold, A., 1955 Physik der Sternatmospheren, 2nd ed. Springer. Berlin.

Vidler M., Tennyson J., 2000, J. Chem. Phys., 113, 9766

Viti S., Jones H. R. A., Maxted P., Tennyson J., 2002, MNRAS, 329, 290

Vrba F.J. et al. 2004, astroph/2272